Soft Matter

The Generic Unfolding of a Biomimetic Polymer during Force Spectroscopy

Journal:	*Soft Matter*
Manuscript ID	SM-ART-12-2019-002545.R1
Article Type:	Paper
Date Submitted by the Author:	09-Mar-2020
Complete List of Authors:	Chaimovich, Aviel; Drexel University, Leitlod, Christian; University of Illinois at Urbana-Champaign Dellago, Christoph; University of Vienna

SCHOLARONE™ Manuscripts

The Generic Unfolding of a Biomimetic Polymer during Force Spectroscopy

Aviel Chaimovich[1a], Christian Leitold[2], and Christoph Dellago[3b]

[1] *Department of Chemical and Biological Engineering, Drexel University, Philadelphia, Pennsylvania 19104*

[2] *Department of Chemical and Biomolecular Engineering, University of Illinois, Urbana, Illinois 61801*

[3] *Faculty of Physics, University of Vienna, 1090 Vienna, Austria*

[a] *aviel.chaimovich@drexel.edu*

[b] *christoph.dellago@univie.ac.at*

Abstract

With the help of force spectroscopy, several analytical theories aim at estimating the rate coefficient of folding for various proteins. Nevertheless, a chief bottleneck lies in the fact that there is still no perfect consensus on how does a force generally perturb the crystal-coil transition. Consequently, the goal of our work is in clarifying the generic behavior of most proteins in force spectroscopy; in other words, what general signature does an arbitrary protein exhibit for its rate coefficient as a function of the applied force? By employing a biomimetic polymer in molecular simulations, we focus on evaluating its respective activation energy for unfolding, while pulling on various pairs of its monomers. Above all, we find that in the vicinity of the force-free scenario, this activation energy possesses a negative slope and a negative curvature as a function of the applied force. Our work is in line with the most recent theories for unfolding, which suggest that such a signature is expected for most proteins, and thus, we further reiterate that many of the classical formulae, that estimate the rate coefficient of the crystal-coil transition, are inadequate. Besides, we also present here an analytical expression which experimentalists can use for approximating the activation energy for unfolding; importantly, it is based on measurements for the mean and variance of the distance between the beads which are being pulled. In summary, our work presents an interesting view for protein folding in force spectroscopy.

1 *Introduction*

The folding of proteins, from expanded coils to collapsed crystals, has been a main research focus for several decades by now [1, 2]. One particularly successful route for studying such a process has been via force spectroscopy: By pulling on a pair of residues of a certain protein, various properties associated with the chain (e.g., the distance between the two beads) can be measured as a function of the applied force [3, 4]. Importantly, the peculiarly rapid folding of a typical protein, to a very low-entropy native state from a very high-entropy chaotic state, is still an unresolved conundrum, and thus, many studies of force spectroscopy especially focus on the kinetic properties of this transition, in both its forward and backward directions [5, 6, 7, 8].

By collecting data at finite forces, while also invoking various analytical theories, a chief aim of the scientific community is in estimating the rate coefficient of the (intrinsic) folding process in the force-free scenario [9]. In an Arrhenius-like manner, the analytical theories generally assume that the activation energy for unfolding is essentially equal, within a constant, to the logarithm of the corresponding rate coefficient. On a phenomenological level, Bell popularized in the biological community a formula, which presumes that the Newtonian work of pulling is entirely absorbed by the activation energy [10]. As an improvement, Dudko et al. presented another analytical expression that notably accounts for the stochastic nature of the folding process via Kramers approach [11]; we sketch the respective activation energy versus the relevant applied force as the blue curve in Fig. 1. Nevertheless, such a kinetic theory is still deficient in describing the empirical behavior of all proteins. Specifically in the vicinity of the force-free scenario, the molecular simulations of Best et al. for ubiquitin showed that the activation energy, as a function of the pulling force, exhibits a negative slope and a negative curvature [12], while the experimental study of Jagannathan et al. for another protein domain reaffirmed this trend [13]; we sketch it as the red curve in Fig. 1. Note that although the Dudko formula also has a negative slope throughout its domain, it possesses the opposite sign for the curvature. It has been argued that the main source for this discrepancy stems from the fact that this analytical theory assumes that the distance between the two beads, on which the force is applied, is always the reaction coordinate for the crystal-coil transition [9]. By assuming that there is just one other component to the reaction coordinate besides the bead-bead distance (e.g., the number of contacts a protein makes with itself), it has been demonstrated that various options for the slope and curvature signs can be obtained [14, 15]. Besides, a generalized approach for the force-free scenario naturally lies in a Taylor expansion for the activation energy: The linear term is basically equivalent with the Bell formula, while the quadratic term accounts for the "compliance" (i.e., an effective compressibility, which is formally defined via the force derivative of the bead-bead distance) [16].

At the most basic level, one may wonder what signs, for the slope and for the curvature, do most proteins exhibit in their force functionality. In other words, given an arbitrary protein, do we know which trend of Fig. 1 it is likely to possess? An ideal model for answering this question is the biomimetic polymer of Taylor et al., which, most notably, is composed of identical beads [17, 18]. By employing the Wang–Landau algorithm [19] for molecular simulations, it was shown that this homogeneous generic polymer mimics the prominent signature of heterogeneous biological polymers: With a particular choice of parameters, this biomimetic chain exhibits a discontinuous (finite-size) phase transition between a collapsed crystal and an expanded coil with no presence of a globule state [17, 18]. Importantly, an ensuing study focused on the force-free kinetics of a slight variant of this polymer, examining many order parameters (e.g., the gyration radius) as possibilities for the reaction coordinate of the crystal-coil transition [20, 21]. Above all, the total potential energy of the chain, in comparison with all other order parameters examined, obtained the best

representation for the reaction coordinate of the folding process. Importantly, the absolute value of this order parameter roughly corresponds with the number of (random) contacts the generic chain makes with itself. This is rather analogous with many kinetic studies which assume that the number of (native) contacts a biological chain makes with itself is a good reaction coordinate for protein folding [22, 23].
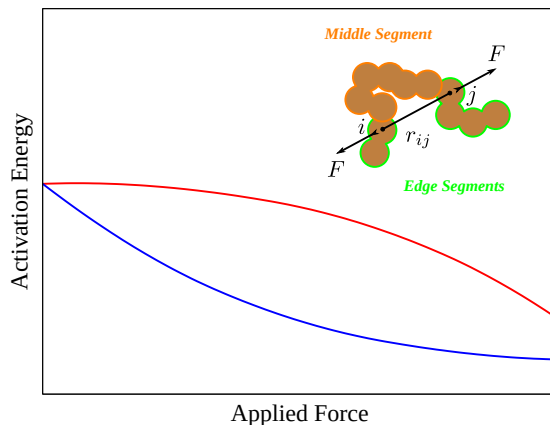

Figure 1: A sketch of the force spectroscopy for a generic unfolding of a biomimetic polymer. The graph plots the two main trends suggested for the activation energy in terms of the applied force (on an arbitrary pair of beads): While both curves have a negative slope throughout their domain, they differ in their curvature, with the blue being convex and the red being concave. Besides, we also have here a schematic which expresses the main notation for the force spectroscopy in our work. The force F is applied between monomers $\{i, j\}$ in the pulling direction of their pairwise distance r_{ij}. In our nomenclature, we call the portion of the chain that is between i and j the middle segment, and the two portions to the left and right of the chain are named the edge segments. In this specific sketch, $N = 12$, with $i = 2$ and $j = 4$, meaning that it is an asymmetric situation in force spectroscopy; the corresponding Δn (i.e., the relative separation in index space) is 7.

Our current work aims at complementing the understanding of the generic crystal-coil transition during force spectroscopy. At the most basic level, via the perturbation theory of Zwanzig [24], we apply a force on an arbitrary monomeric pair of the biomimetic polymer studied by the molecular simulations of Refs. [20, 21]. Reminiscent of the various theories for force spectroscopy [9], we aim at clarifying transition kinetics by focusing here on free energies: The main assumption of our study is that the total potential energy of the polymer is an adequate approximation for the reaction coordinate of the crystal-coil transition. We consequently show, for generic unfolding, that its activation energy in the force-free limit consistently exhibits a negative slope and a negative curvature as a function of the applied force, which is in line with findings for ubiquitin [12], as well as for other protein domains [13]. Our work thus suggests that most proteins exhibit such a a functionality in force spectroscopy, and that other trends are exceptions to this general rule.

2 *Polymer System*

As mentioned earlier, the basis for our biomimetic polymer is the model of Taylor et al. [17]; a schematic of an arbitrary configuration of such a chain is given in the inset of Fig. 2. We specifically use the singularity-free version of this model devised in Ref. [20] for purposes of studying the kinetic behavior of the polymer (its

equilibrium phenomena is essentially identical with that of the original model). Depicted in Fig. 2 as the black curve, the pairwise potential u between non-neighboring beads is a function of their pairwise distance r, and it is given by [20]:

$$u\left(r\right) = \frac{1}{2}\epsilon\left[\exp\left[-\alpha\left(r/\sigma - 1\right)\right] + \tanh\left[\alpha\left(r/\sigma - \lambda\right)\right] - 1\right] \tag{1}$$

The spatial parameter σ is the width of the wall-like core, and the energetic parameter ϵ is the depth of the square-like well; our entire study is made dimensionless in terms of these two. The dimensionless λ controls the diameter of the latter: We fix it at $\lambda = 1.05$, since this is a value which can attain the aforementioned crystal-coil transition (i.e., a chief characteristic of protein folding); note that this value makes the attractive well very narrow compared to the repulsive core. The tuning parameter α regulates the smoothness of this function, and we fix it at $\alpha = 500$. Furthermore, depicted in Fig. 2 as the gray curve, the harmonic bonds of this polymer are governed by [20]:

$$u\left(r\right) = \frac{1}{2}\epsilon\kappa\left(r/\sigma - 1\right)^2 \tag{2}$$

The dimensionless spring constant κ is set to $20,000$. Besides, we set the number of monomers N to 128. Note that $\alpha \to \infty$, together with $\kappa \to \infty$, retrieves the original model of Taylor et al. [17].
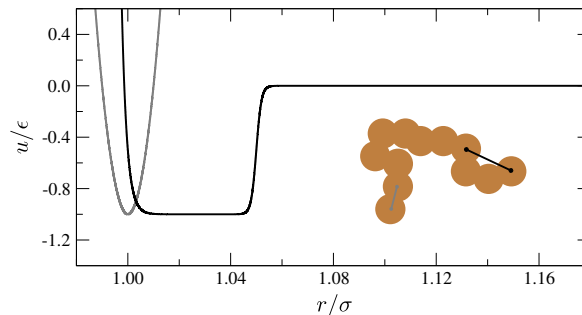

Figure 2: The model of the biomimetic polymer of identical beads. Besides the schematic of the chain, we also present here the pairwise potential in terms of the pairwise distance. The black curve is relevant for non-neighboring beads: It is the singularity-free version of a wall-like core with a square-like well given by Eq. 1. The gray curve is the harmonic bond of Eq. 2; for clarity, it is shifted downwards by unity.

Given the positions of all monomers r^N, the total potential energy of the chain U is defined by the pairwise summation of Eq. 1, together with that of Eq. 2. Once a force is applied between an arbitrary pair of beads i and j, the configurational Hamiltonian of the system H_F is given by:

$$H_F\left(r^N\right) = U\left(r^N\right) - Fr_{ij} \tag{3}$$

Here, r_{ij} is the scalar distance between the two relevant monomers (its trivial dependence on r^N is omitted for clarity), while F is the scalar force, defined in the pulling direction of r_{ij}. Note that for the force-perturbed system, H_F is the total potential energy, not just U. Our corresponding notation for the bead indices is the following: The index i or j is the ordinal number of the monomer counting from the leftmost or rightmost edge, respectively. As a clarification, the symmetric scenario corresponds with $i = j$; for example,$\{i, j\} = \{1, 1\}$ means the force is applied on the edge beads, while $\{i, j\} = \left\{\frac{1}{3}\left(N + 1\right), \frac{1}{3}\left(N + 1\right)\right\}$ is the case in which the polymer is partitioned into three equal segments. We frequently call the polymeric

portion between the $\{i, j\}$ monomers as the middle segment, while the other two portions are referred to as the edge segments. We also define their corresponding separation in index space:

$$\Delta n = N - (i + j) + 1 \tag{4}$$

This notation is sketched in Fig. 1.

Importantly, note that specific values of the configurational functions which appear in Eq. 3 can be used as order parameters (e.g., a bead-bead distance r_{ij}). In our work, the most important order parameter which we examine is U. Above all in the force-free study of Taylor et al., it was shown that the total potential energy can clearly discriminate between the collapsed and expanded states of their biomimetic polymer [17]. As we alluded to earlier, $-U/\epsilon$ is fairly representative of the number of contacts that the monomers make with each other, since Eq. 1 is almost binary in its functionality, with its dimensionless version being essentially 1 or 0 depending on whether a contact is established or removed, respectively. In turn, the collapsed state has many contacts with a large $|U|$, and the expanded state has few contacts with a small $|U|$ (a representative schematic can be found in Fig. 3). In consideration of our dimensionless study, we frequently refer to $|U|$ (sometimes even colloquially to U itself) as the "contacts-number". On a relevant note, we generally use $\mathcal{A}$ and $\mathcal{B}$ as labels for the crystal and coil states, respectively, while a double dagger ‡ is employed for referring to the transition region between these two metastable phases.

3   *Molecular Simulations of the Force-Free Scenario*

Examining both the crystal and coil phases of the polymer, especially the folding process, is rather cumbersome: A regular molecular simulation would spend most of its time in one of the phases, and it would rarely make the transition between the two. This bottleneck can be overcome via the Wang–Landau algorithm, which iteratively evaluates the density of states of the system, while also generating a respective flat histogram for the ensemble of configurations in terms of the total Hamiltonian energy as the order parameter [19]. Still, the Wang–Landau strategy is quite expensive computationally, and thus in our specific study, instead of performing the algorithm for various force values, as well as for various bead pairs, we essentially execute it only for the special case of $F = 0$; for treating force spectroscopy, we employ the perturbation theory of Zwanzig [24], which is thoroughly discussed in a later section below. Regardless, the molecular simulations of the biomimetic polymer in the force-free scenario are essentially the basis for all of the data presented here.

In the absence of a force, the total Hamiltonian energy is identical with the total potential energy (i.e., $H_0 = U$), and in turn, the Wang–Landau approach, via the density of states Ω_0, conveniently provides the corresponding (canonical) probability distribution $\mathcal{P}_0$,

$$\mathcal{P}_0(U) = \Omega_0(U) \exp\left[-U/kT\right]/Z_0 \tag{5}$$

in which Z_0 is the (canonical) partition function; k is the Boltzmann constant, while T is the temperature of interest. Within an arbitrary constant, the respective free energy G_0 is given by the logarithm of the above;

$$G_0(U) = -kT \ln \Omega_0(U) + U + \text{cnst.} \tag{6}$$

5

throughout this publication, we choose the arbitrary constant so that the folded state has zero energy. We also restrict our current work to the coexistence temperature between the crystal and coil phases at $F = 0$: This corresponds with $kT = 0.438\epsilon$ [20]. We show the corresponding free energy (as the black curve), together with the probability distribution (as the gray curve), in Fig. 3. It is now obvious that the two metastable phases are separated by a rare transition region. Throughout our work, we define the crystal $U^{\mathcal{A}}$ and the coil $U^{\mathcal{B}}$ as the values of the order parameter which correspond with the minima in the free energy. Analogously, we also denote $U^{\ddagger}$ as the value of the "contacts-number" associated with the maximum in the free energy. For this force-free scenario, $U^{\mathcal{A}} \approx -367\epsilon$ and $U^{\mathcal{B}} \approx -57\epsilon$, while at the same time, $U^{\ddagger} \approx -179\epsilon$.

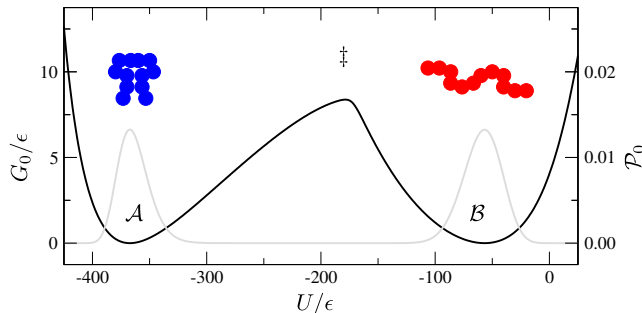Figure 3: The force-free transition between the crystal and coil phases at the temperature of coexistence (i.e., $kT = 0.438\epsilon$). Plotted in terms of the "contacts-number" as the order parameter, the black curve is the free energy (on the left ordinate), while the gray curve is the probability distribution (on the right ordinate); the arbitrary constant of the former is chosen so that the metastable phases have a value of zero. The left and right schematics correspondingly depict the collapsed and expanded states.

The probability distribution of Eq. 5, together with all the configurations generated by the molecular simulations, can be employed for reweighing any property of the polymer at U into the equivalent property at T. The reweighing of an average of an arbitrary configurational function $\psi\left(r^{N}\right)$ can be numerically determined via the following integration over the order parameter:

$$\langle\psi\rangle_0 = \int \langle\psi\rangle_0^U \, \mathcal{P}_0\left(U\right) dU \tag{7}$$

The brackets here mean ensemble averaging: The presence of the index U corresponds with averaging at that particular value of the "contacts-number"; if this index is absent, canonical averaging at T is implied. Note that there is another version of this expression based on the delta function: $\langle\delta\left(U\right)\psi\rangle_0 = \langle\psi\rangle_0^U \, \mathcal{P}_0\left(U\right)$; $\delta\left(U\right)$, in the brackets, is an abbreviated notation for the familiar delta function, $\delta\left(\hat{U}\right) = \delta\left(\hat{U} - U\left(r^{N}\right)\right)$, with its dependence on the positions of all beads implied.

We briefly describe our current implementation of the Wang–Landau algorithm, which is equivalent with the one of Ref. [20]. The molecular simulations evolve via Monte Carlo moves: Besides the standard single-particle displacement, there are four special types of polymeric moves, which are randomly executed half of the time (on average). One pass of the simulations consists of $2N = 256$ moves. Using the already converged density of states calculated in Ref. [20], we examine the order parameter U over two windows, $[-430\epsilon, -70\epsilon]$ and $[-70\epsilon, 130\epsilon]$, using a bin size of 1ϵ. We record the positions of all monomers every 10^5 passes, which ensures that any two configurations are completely decorrelated from each other. Conventional rules for modification factors, as well as for histogram flatness, are employed. We perform 16 sets of this algorithm in parallel, and we eventually combine all of their data together. For any given U, we harvest

about $4,000$ uncorrelated configurations of the polymer.

4   *Pairwise Distance between Two Monomers*

The probability distribution for U of Fig. 3, which is directly generated by the Wang–Landau algorithm, can be reweighed to a probability distribution for any other order parameter. In particular, let us consider an arbitrary pairwise distance r_{ij} (at this point, there is still no force between beads i and j). Remember that this is an order parameter which is frequently assumed as a reaction coordinate in many kinetic theories for protein folding [11]. We consequently substitute the delta function $\delta\left(r_{ij}\right)$ for ψ in Eq. 7, attaining the following:

$$\mathcal{P}_0\left(r_{ij}\right) = \int \mathcal{P}_0^U\left(r_{ij}\right)\mathcal{P}_0\left(U\right) dU \tag{8}$$

Note that $\mathcal{P}$ with an extra index U (i.e., $\mathcal{P}_0^U$) corresponds to a conditional distribution at that value of the "contacts-number"; the absence of such an index means that a probability distribution is canonical at T. Employing the many Wang–Landau configurations, we numerically evaluate this probability distribution: For a given bead pair $\{i, j\}$, we construct a histogram in terms of their r_{ij} at a specific U, and by running across this entire order parameter, while also using its (canonical) probability distribution $\mathcal{P}_0\left(U\right)$, we correspondingly obtain the (canonical) probability distribution for the pairwise distance $\mathcal{P}_0\left(r_{ij}\right)$.
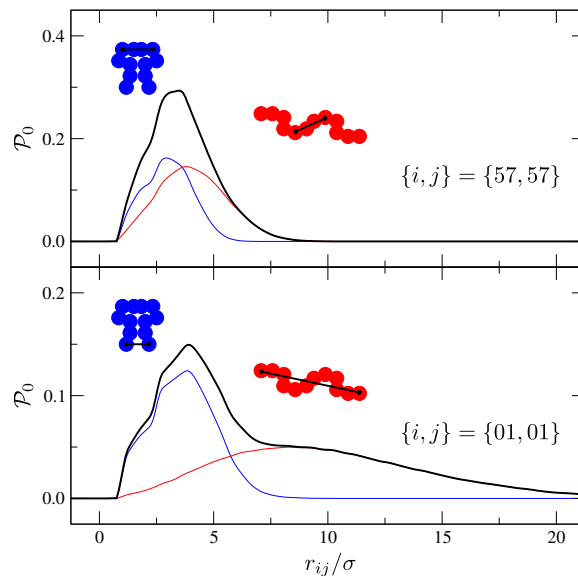

Figure 4: The probability distribution for the pairwise distance between a bead pair in the force-free scenario. The panels only differ in terms of their specific monomeric pair, with the top being for $\{i, j\} = \{57, 57\}$ and the bottom being for $\{i, j\} = \{01, 01\}$; notice that the ordinate-axis differs by a factor of two. The black curve is the probability distribution across all of U. The colored curves are probability distributions for restricted regions of the "contacts-number": Specifically represented by their corresponding schematics, the blue and red curves are for the crystal and coil states, respectively.

In Fig. 4, we present this probability distribution as the black curve for two sets of bead pairs, with

the top panel for $\{i,j\} = \{57,57\}$ and the bottom panel for $\{i,j\} = \{01,01\}$; realize that the top range is twice as much as the bottom range. The noticeable difference between the two panels is associated with the overall monotonic relationship between the bead separation in index space and the bead separation in real space: Larger Δn generally involves larger r_{ij}, and thus, the probability distribution has higher values in the top panel than in the bottom panel. Besides this numerical discrepancy, the common aspect in both panels is that this $\mathcal{P}$ does not at all exhibit two clearly separated hills (compare with the probability distribution of Fig. 3). This means that r_{ij} is not an adequate order parameter for distinguishing between the crystal and coil phases, which in turn implies that it cannot be the reaction coordinate!

Let us clarify the situation here. We can partition the overall $\mathcal{P}$ into its two main contributions, one around the crystal basin, $U/\epsilon = [-402, -302]$ and one around the coil basin $U/\epsilon = [-114, -14]$; these boundaries for U are chosen so that each metastable phase corresponds with a G_0 that is roughly within $5kT$ of its basin. Labeled by the colored schematics, the separate crystal and coil contributions to the entire probability distribution are given respectively as the blue and red curves in Fig. 4. Due to the low probability of finding the system outside of the stable basins, the sum of the two curves is almost identical with the black curve. It is now clear that there is a significant overlap between the separate probability distributions of the crystal and coil phases: While r_{ij} is quite small for the crystal and quite large for the coil, this plain two-body property can fluctuate considerably for each of the metastable phases, and it cannot describe the collective multi-body transition of the entire polymer. This overlap is consequently the source for the inadequacy of r_{ij} as an order parameter.

In line with our generic polymer, other recent studies also suggest that the pairwise distance between arbitrary beads cannot be generally presumed as the reaction coordinate for the crystal-coil transition [9]. Nevertheless, this may not be necessarily the case for protein folding. Since a biological chain folds in a very unique manner, its probability distribution for a pairwise distance is much sharper, and it can also involve many other basins. In turn, a given protein may have a certain r_{ij} that cleanly distinguishes between the collapsed and expanded phases, while also playing a key role in the reaction mechanism.

5 Application of a Force between Two Monomers

We again emphasize that the focal part of the current work is in mimicking force spectroscopy, specifically examining the influence of an applied force F (between an arbitrary bead pair $\{i,j\}$) on the free energy G_F of our generic chain, in terms of the "contacts-number" U as the order parameter. While for lattice systems, such a calculation may be feasible by the direct application of the Wang-Landau algorithm [25], this may not be the case for our polymeric model. In turn, rather than performing the Wang–Landau algorithm for many values of F (with numerous sets of $\{i,j\}$), we go about this task via a rather computationally inexpensive route, which is based on the perturbation theory of Zwanzig [24]. With the force-free chain being the reference system in the Zwanzig formalism, the applied force is the perturbation parameter which changes the total Hamiltonian energy from H_0 to H_F. Given an arbitrary configurational function $\psi\left(r^N\right)$, Zwanzig perturbation means the following for Eq. 3:

$$\langle\psi\rangle_F = \langle\psi \exp\left[Fr_{ij}/kT\right]\rangle_0 \, / \, \langle\exp\left[Fr_{ij}/kT\right]\rangle_0 \tag{9}$$

In line with the notation of the zero index above (e.g., $\langle\psi\rangle_0$), the F index denotes the value of the force which corresponds with the appropriate ensemble average. Substituting the delta function $\delta(U)$ for ψ in the above yields:

$$\mathcal{P}_F(U) = \mathcal{P}_0(U)\langle\exp[Fr_{ij}/kT]\rangle_0^U / \langle\exp[Fr_{ij}/kT]\rangle_0 \tag{10}$$

Note that we also invoke here the infinitesimal version of Eq. 7 with $\psi = \exp[Fr_{ij}/kT]$. We consequently have the respective free energy,

$$G_F(U) = G_0(U) - kT\ln\langle\exp[Fr_{ij}/kT]\rangle_0^U + \text{cnst.} \tag{11}$$

with an arbitrary constant (independent of U but not of F), which is again set at a value that ensures $G_F = 0$ for the folded state. We emphasize here that the entire formalism (e.g., Eqs. 5, 7, 9, 11, etc.) is completely universal. As such, all expressions above can be employed in examining any protein; the only unique feature that one must consider is the specific model used for H_0, and this may also influence the exact choice for the order parameter of the crystal-coil transition.
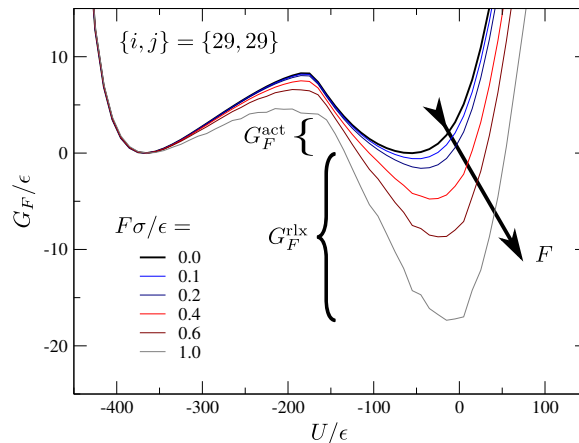

Figure 5: The free energy as a function of the "contacts-number", while varying the magnitude of the applied force. Each curve corresponds to a different value of the force. The black one is actually for the force-free scenario, and it is identical with its counterpart in Fig. 3. The other colored curves correspond with the polymer under force spectroscopy: The arrows mean that the value of the force increases, and in this graph, it is always applied between monomers $\{29, 29\}$. Besides, we schematically depict here the activation and relaxation energies associated with the gray curve (i.e., the case of $F = 1.0\epsilon/\sigma$).

We now specifically apply the above formalism on our polymer. We numerically loop over all U for a particular bead pair $\{i, j\}$: At a specific U, we essentially run over all of the relevant (force-free) Wang–Landau configurations, averaging for them $\exp[Fr_{ij}/kT]$, simultaneously for many values of F. Note that because the exponential factor is an increasing monotonic function of Fr_{ij}, this perturbation term naturally generates noticeable statistical uncertainty for the unfolded state around $F \approx 1\epsilon/\sigma$ (in comparison with the folded state around $F \approx 0\epsilon/\sigma$); for alleviating this issue, we average, upon the completion of the protocol, all of our data by lumping U in bins of 10. Besides, in line with other sections of this publication, we only perform this procedure at the coexistence temperature of the force-free scenario; realize, of course, that upon (finite) force spectroscopy, the crystal and coil metastable phases are not at coexistence anymore. Such a Zwanzig

protocol has negligible computational cost compared to the Wang–Landau algorithm, and thus it is rather trivial to perform the Zwanzig calculation for many different bead pairs.

Consider the specific monomeric pair $\{29, 29\}$: This is a symmetric scenario for force spectroscopy, in which the two edge segments are (roughly) a quarter of the total polymeric length, while the middle segment is the remaining (roughly) half of the polymer. For this set of beads, we present its free energy as a function of the "contacts-number" in Fig. 5, while varying the magnitude of the applied force. The black line is for the force-free scenario, which is basically identical with the analogous curve of Fig. 3; all other colors correspond with different values of a (finite) force. As expected, increasing the magnitude of the pulling force (represented by the arrow) makes the transition from the crystal to the coil more and more favorable: The change in the free energy between the two metastable states increases (in terms of its absolute value), and this occurs concurrently with a decreasing barrier for unfolding.
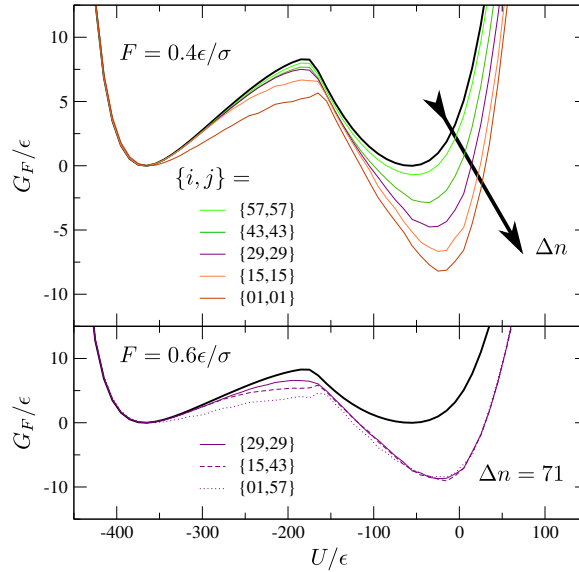

Figure 6: The free energy as a function of the "contacts-number", with the force applied on various monomeric pairs. The top panel examines $F = 0.4\epsilon/\sigma$, and it is only for symmetric scenarios, in which the length of the middle portion, in index space, is varied, while its midpoint is fixed at the center of the polymer; the arrow corresponds with an increase in this length, and the color of a curve determines the respective value. The bottom panel examines $F = 0.6\epsilon/\sigma$, and it is only for asymmetric scenarios, in which the middle segment of the polymer is always the same length in index space (i.e, 71), while the corresponding location of its midpoint is varied.

Let us now fix the force at a constant value, while varying the beads on which it is applied. In the top panel of Fig. 6, with $F = 0.4\epsilon/\sigma$, we specifically examine symmetric scenarios of force spectroscopy: The two edge segments are always equal in length, while we just vary the relative separation, in index space, between the two monomers (i.e., Δn). Interestingly, varying this parameter gives a trend analogous with the one mentioned above in the context of Fig. 5: With increasing Δn, as well as with increasing F, G_F shifts to lower values across its entire order parameter (considering our choice for the arbitrary constant). This correspondence of Δn with F stems in the monotonic relationship between the bead separation in index space and the bead separation in real space, discussed in the context of Fig. 4: Since r_{ij} has the same functionality as F in the Zwanzig factor (i.e., $\exp[Fr_{ij}/kT]$), increasing this pairwise distance should have

10

the same general effect as amplifying the magnitude of the applied force. On the other hand, the bottom panel of Fig. 6 presents several asymmetric scenarios for $F = 0.6\epsilon/\sigma$; while the two edge segments are not of the same length here, they are of the same family in the sense that Δn is fixed between them. Interestingly, for such a family of curves, the difference in free energy between the two metastable phases is essentially unperturbed, while the barrier for unfolding noticeably changes. Overall, it is clear that there are subtle effects on G_F across its order parameter, depending on which specific beads the force is applied.

6   *Moments of the Pairwise Distance*

Let us now switch back our focus to the other order parameter that we explore in this publication (the reason for this will become clear in the next section). Specifically, we examine moments of the pairwise distance between an arbitrary monomeric pair; this essentially corresponds with the moments of the probability distributions of Fig. 4, except that we now vary the applied force. We focus on the first and second moments, which allow us to obtain mean and variance of the pairwise distance. The moments can be calculated by setting ψ equal to different powers of r_{ij} in Eq. 9, together with Eq. 7. We implement this computation in the numerical script described in the previous section. We plot in the top and bottom panels of Fig. 7 the respective mean $\langle r_{ij} \rangle_F^U$ and variance $\langle \Delta r_{ij}^2 \rangle_F^U$ as a function of the "contacts-number"; we introduce here $\Delta r_{ij} = r_{ij} - \langle r_{ij} \rangle_F^U$, with the dependence of the delta symbol on the indices (e.g., F) being implicit. The coding here is analogous with the one in Fig. 5: The different colors are for the same values of the force, which is again applied on $\{i, j\} = \{29, 29\}$.

For the $F = 0$ case (i.e., the black curves), the trend is the same for both moments: As expected, they are both low for the (rigid) crystal, and they are both high for the (floppy) coil. While this function is almost monotonic throughout, there is a slight inflection in the transition region (i.e., at $U \approx -200\epsilon$), which corresponds with the location of the barrier in the free energy. Taylor et al. noticed an analogous behavior for the gyration radius [18], and overall, this may correspond to a subtlety in the nucleation process: As the biomimetic polymer transitions from a crystal to a coil, there is an instance during which various of its contacts are broken, yet its size contracts. On a related note, the string analysis of Ref. [21] observed a switch in the main contribution to the reaction coordinate (i.e., from "contacts-number" to "crystallinity") around the same location of U. \

Once a force is applied, we observe completely different behavior between the mean and the variance. The relationship for $\langle r_{ij} \rangle_F^U$ is quite simple, with a stronger force yielding a larger mean. Nevertheless, the situation is rather complex for $\langle \Delta r_{ij}^2 \rangle_F^U$, being notably non-monotonic: At a high "contacts-number" (e.g., $-U/\epsilon \approx 300$), the variance generally increases with F, yet at a low "contacts-number" (e.g., $-U/\epsilon \approx -100$), the variance generally decreases with F. Besides, it seems that both moments reach an asymptote at $F = 1.0\epsilon/\sigma$, since they do not change much beyond this value. Here is how one can understand the situation. As we pull stronger and stronger on the crystal state, it disentangles, with the beads getting farther apart, while fluctuating more on its periphery. On the other hand, as we pull stronger and stronger on the coil state, the beads very easily stretch out between each other, and being very stretched, they do not have much of a possibility for fluctuations.
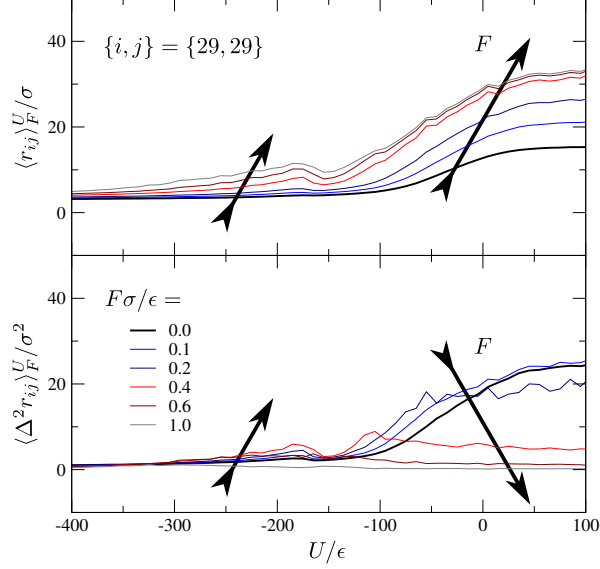
Figure 7: The moments of the pairwise distance as a function of the "contacts-number". The top panel is for the mean, and the bottom panel is for the variance. The color coding here for the applied force, on beads $\{29, 29\}$, is identical with the one in Fig. 5, and again, the arrows denote the general trend for an increasing force.

7   Approximations for Force Spectroscopy

For various reasons, one may be interested in estimating the approximate effect of force spectroscopy on a certain polymer. For example, one can solely perform a molecular simulation of a force-free scenario of a protein, while subsequently predicting the free energy for a finite force; conversely, experiments can be done at a finite force, while estimating the free energy for the force-free case.

As such, we correspondingly formulate a Taylor series for $G_F(U)$ in the vicinity of $F = 0$. In consideration of Eq. 11, here is its first-order derivative,

$$\frac{\partial}{\partial F} G_F(U) = -\frac{\langle r_{ij} \exp\left[Fr_{ij}/kT\right]\rangle_0^U}{\langle \exp\left[Fr_{ij}/kT\right]\rangle_0^U}$$

$$\left[\frac{\partial}{\partial F} G_F(U)\right]_{F=0} = -\langle r_{ij}\rangle_0^U \tag{12}$$

and here is its second-order derivative,

$$\frac{\partial^2}{\partial F^2} G_F(U) = -\frac{1}{kT}\left(\frac{\langle r_{ij}^2 \exp\left[Fr_{ij}/kT\right]\rangle_0^U}{\langle \exp\left[Fr_{ij}/kT\right]\rangle_0^U}\right) + \frac{1}{kT}\left(\frac{\langle r_{ij} \exp\left[Fr_{ij}/kT\right]\rangle_0^U}{\langle \exp\left[Fr_{ij}/kT\right]\rangle_0^U}\right)^2$$

$$\left[\frac{\partial^2}{\partial F^2} G_F(U)\right]_{F=0} = -\frac{1}{kT}\langle \Delta r_{ij}^2\rangle_0^U \tag{13}$$

both evaluated at $F = 0$. Combining these two, we have an approximation for the free energy during force

spectroscopy:

$$G_F\left(U\right) \approx G_0\left(U\right) - \left\langle r_{ij}\right\rangle_0^U F - \frac{1}{2}\frac{1}{kT}\left\langle\Delta r_{ij}^2\right\rangle_0^U F^2 + \ldots + \mathrm{cnst.} \tag{14}$$

These perturbation terms for the free energy in the force-free case (i.e., $G_0\left(U\right)$) have a very simple meaning: During force spectroscopy in the vicinity of $F = 0$, the mean $\left\langle r_{ij}\right\rangle_0^U$ corresponds with the slope of $G_F\left(U\right)$, and the variance $\left\langle\Delta r_{ij}^2\right\rangle_0^U$ corresponds with the curvature of $G_F\left(U\right)$.
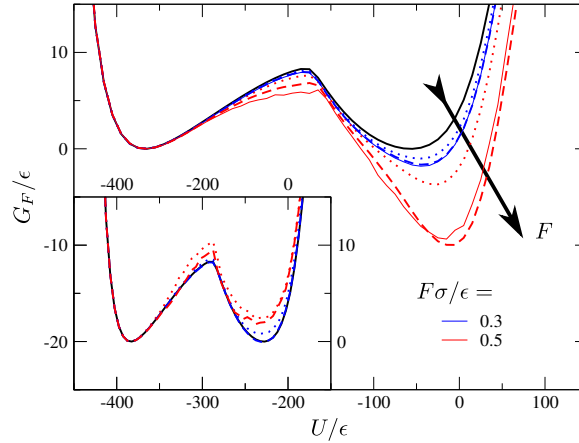

Figure 8: Approximations for the free energy as a function of the "contacts-number". Besides the free energy for $F = 0$ (i.e., the black curve), there are two sets of colored curves here corresponding with two different cases of force spectroscopy: The blue lines are always associated with a force of $0.3\epsilon/\sigma$ on beads $\{43, 43\}$ ($\Delta n = 43$), and the red lines are are always associated with a force of $0.5\epsilon/\sigma$ on beads $\{15, 15\}$ ($\Delta n = 99$); note that the arrow denotes an increasing value of the force, as well as of the relative separation in index space. In the main panel, while all solid lines are the exact free energies given by Eq. 11, the other curves represent their respective approximations via the Taylor series of Eq. 14: The dotted lines just use the linear term, while the dashed lines also use the quadratic term. Conversely, the auxiliary panel focuses on estimating the free energy at $F = 0$ by invoking Eq. 15: Again, the dotted and dashed lines respectively correspond with linear and quadratic approximations.

Eq. 14 is completely general, and we now examine its efficacy in describing the free energy of our polymer. Importantly, considering the black curves in Fig. 7, together with the black curve for $G_0\left(U\right)$ (the one which frequently appears in our graphs), we have already presented all the necessary ingredients for this computation. In the main panel of Fig. 8, we consequently present two sets of perturbations: The blue curves are for a small perturbation (i.e., $F = 0.3\epsilon/\sigma$ on beads which are near to each other with $\Delta n = 43$), and the red curves are for a large perturbation (i.e., $F = 0.5\epsilon/\sigma$ on beads which are far from each other with $\Delta n = 99$). While the solid curves are for the exact free energies by Eq. 11, the first-order and second-order approximations, based on the Taylor expansion of Eq. 14, are respectively given as dotted and dashed curves. Naturally, for a fairly small force, just the slope at $F = 0$ is sufficient, yet for a fairly large force, also the curvature at $F = 0$ is necessary. In any case, we can state that by employing the two terms given in the Taylor series above (i.e., in Eq. 14), we can generally capture the functionality of the free energy of our polymer in force spectroscopy.

Nevertheless, in experiments of force spectroscopy, the opposite situation is usually the case: Measurements are made at a finite F, and estimates for $G_0\left(U\right)$ are desired. As such, two other Taylor approximations are required for that, specifically, for the moments of the pairwise distance which appear in Eq. 14. Follow-

ing an analogous approach as in Eqs. 12 and 13, $\langle r_{ij}\rangle_F^U \approx \langle r_{ij}\rangle_0^U + \frac{1}{kT}\langle\Delta r_{ij}^2\rangle_0^U F$ and $\langle\Delta r_{ij}^2\rangle_F^U \approx \langle\Delta r_{ij}^2\rangle_0^U$.
Making the appropriate substitutions in Eq. 14, together with some rearrangement, we obtain the following:

$$G_0\left(U\right) \approx G_F\left(U\right) + \langle r_{ij}\rangle_F^U F - \frac{1}{2}\frac{1}{kT}\langle\Delta r_{ij}^2\rangle_F^U F^2 + \ldots + \text{cnst.} \tag{15}$$

Essentially, this expression is almost identical with Eq. 14, except that one of the terms has its sign switched.

We consequently present in the auxiliary panel of Fig. 8 estimates for the free energy of the force-free scenario (i.e., the black curve). The coloring here is analogous with that of the main panel: The blue curves use the Zwanzig data of $F = 0.3\epsilon/\sigma$ with $\Delta n = 43$, and the red curves use the Zwanzig data of $F = 0.5\epsilon/\sigma$ with $\Delta n = 99$; again, the dotted and dashes lines respectively correspond with the linear and quadratic approximations of Eq. 15. The approximations here are not quite as successful as those of the main panel: Good agreement is only seen for small perturbations, and even then we have to include both the linear as well as the quadratic term in the expansion. This is perhaps due to the fact that extra approximations were introduced for Eq. 15 (i.e., for $\langle r_{ij}\rangle_F^U$ and $\langle\Delta r_{ij}^2\rangle_F^U$). Overall, this auxiliary panel of Fig. 8 conveys the fact that if one is interested in estimating the force-free G_0 experimentally, one must generally aim for measurements at small forces, as well as with small Δn, and we also strongly recommend employing both terms in the Taylor series for a better approximation.

8   *Activation Energy of the Crystal-Coil Transition*

We now finally connect our current equilibrium study for free energies of generic polymers with the various kinetic studies of protein folding. As alluded to earlier, we do so with one crucial assumption: The "contacts-number" is a decent approximation for the ideal reaction coordinate of the unfolding process. We can presume this with relative confidence since Refs. [20, 21] found that the "contacts-number" gives the best correspondence with the committer probability (in comparison with many other order parameters), and besides, many kinetic studies of protein folding do actually employ the "contacts-number" for their reaction coordinate.

With this presumed choice for the reaction coordinate, the activation energy G_F^{act} for the crystal-coil transition is defined as follows:

$$G_F^{\text{act}} = G_F\left(U^{\ddagger}\right) - G_F\left(U^{\mathcal{A}}\right) \tag{16}$$

We depict it schematically in Fig. 5; realize that the locations of the extrema (e.g., $U^{\ddagger}$) are implicitly dependent on F. By enumerating these points in our curves (e.g., those in Fig. 5), we evaluate the activation energy, and we present it as a function of the applied force, in Fig. 9. Each curve here is for a different bead pair in force spectroscopy, with the top and bottom panels respectively being for symmetric and asymmetric pulling. In terms of the dependence on the bead pair, we make analogous observations as we made in the context of Fig. 6: In the top panel, we note that the activation barrier decreases as the relative separation (in index space) increases, and in the bottom panel, we observe that the equivalent effect can be achieved by pulling on a segment at the edge of the polymer rather than at the middle of the polymer. Regardless, the striking signature of Fig. 9 is that all the different curves exhibit almost the same functionality with F: Originating at the value of the activation energy for the force-free scenario (i.e., $G_0^{\text{act}} = 8.28\epsilon$), they all

posses a negative slope and a negative curvature (at least for moderate forces below $1\epsilon/\sigma$). Note that this is reminiscent with our observations for the free energy over the entire order parameter in the specific case of $\{i,j\} = \{29, 29\}$ in Fig. 5.
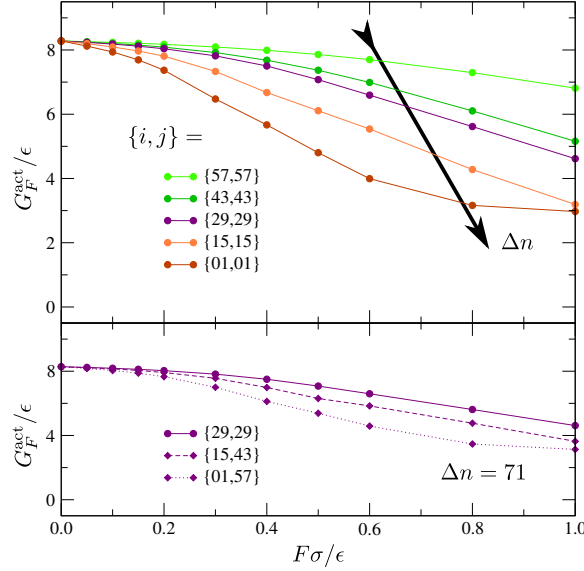

Figure 9: The activation energy as a function of the applied force. The coding here is reminiscent of Fig. 6. In the top panel, the different colors correspond with various separations between the bead pair; the arrow means increasing Δn; conversely, the bottom panel maintains a constant Δn. The circles, connected by solid lines, are for symmetric scenarios, and the diamonds, connected by broken lines, are for asymmetric cases.

Why do we observe this generic functionality in force spectroscopy regardless of which monomeric pair F is applied on? To answer this question, we substitute the Taylor approximation of Eq. 14 in the definition of Eq. 16, obtaining the following series for the activation energy in terms of the applied force:

$$G_F^{\text{act}} \approx G_0^{\text{act}} - \left[\langle r_{ij} \rangle_0^{\ddagger} - \langle r_{ij} \rangle_0^{\mathcal{A}} \right] F - \frac{1}{2} \frac{1}{kT} \left[\langle \Delta r_{ij}^2 \rangle_0^{\ddagger} - \langle \Delta r_{ij}^2 \rangle_0^{\mathcal{A}} \right] F^2 + \ldots \tag{17}$$

Importantly, we find that the slope and the curvature of the activation energy are given as the differences between the means and the variances, respectively, evaluated at the appropriate extrema of $F = 0$. Note that this expression is in effect a variation on the recent extension of the Bell model: The linear term is the main aspect of the original expression, while the quadratic term is an improvement that accounts for the "compliance" [16]. Specifically for the bead pair $\{29, 29\}$, we examine the efficacy of this expression in the top panel of Fig. 10. The violet circles are identical with their counterparts in Fig. 9; the dotted and dashed curves are respectively the first-order and second-order approximations based on the Taylor series of Eq. 17. As can be clearly noticed, with a negative slope and a negative curvature across all F, the quadratic approximation captures the general functionality of the exact curves very well (the linear approximation is inherently deficient in doing so). Note that we observe analogous trends for other bead pairs as well.

Considering the approximation of Eq. 17, the functionality of the free energy for our biomimetic chain now makes perfect sense. According to Fig. 7, $\langle r_{ij} \rangle_0$ and $\langle \Delta r_{ij}^2 \rangle_0$ are fairly negligible in the folded state, yet they become relatively noticeable across the transition region. This makes the corresponding differences between the moments in Eq. 17 positive, thus yielding a negative slope and a negative curvature for the

curves of Fig. 10. We suspect that most proteins have such a signature. This is because in general, the folded state is always compact with a stiff structure, and upon disentanglement, the overall size increases together with the respective fluctuations; in other words, a distance between an arbitrary residue pair in a certain protein usually possesses the $F = 0$ trend of Fig. 7. Nevertheless, some proteins may exhibit a different functionality for G_F^{act}, particularly because some of their residues have specific preferences for each other. For example, if the fluctuations in r_{ij} significantly diminish across the transition region (perhaps because the two relevant residues must adhere to certain portions of the protein so that unfolding occurs), force spectroscopy will exhibit the functionality of the blue curve of Fig. 1. Realize that other peculiar trends in protein unfolding have been noted as well (e.g., the activation energy initially increases at $F = 0$) [9]. In any case, a given protein may only have a few special pairs that play a pivotal role in the crystal-coil transition. Thus in most cases, if one applies a force on a random pair of residues in a certain protein, the functionality of the red curve in Fig. 1 is expected in the vicinity of $F = 0$.
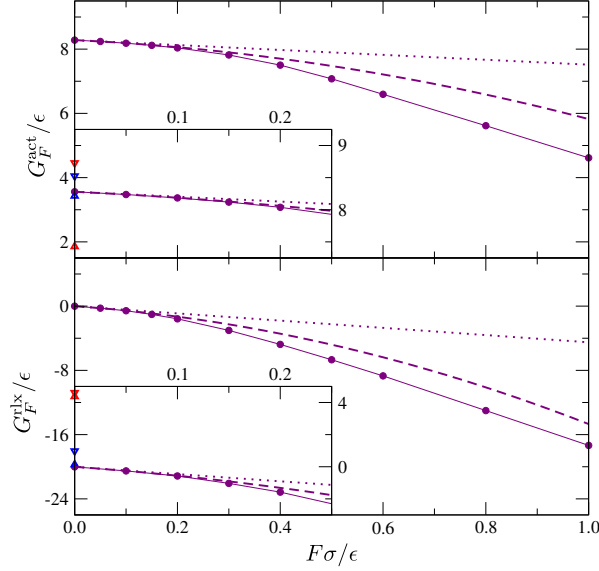

Figure 10: Estimates for changes in the free energy as a function of the applied force. The top panel is for the activation energy, and the bottom panel is for the relaxation energy. Specifically for the bead pair $\{29, 29\}$, the violet circles are the exact data, with the line between them just serving as a guide; the dotted and dashed lines correspond with the first-order and second-order approximations, respectively, given by Eq. 17. The auxiliary panels focus on the curves in the vicinity of the force-free scenario. Here, we also plot points on the ordinate-axis, which correspond with estimates for the free energies at $F = 0$: Specifically, the down and up triangles respectively represent the linear and quadratic approximations of Eq. 18; corresponding with the Zwanzig curves of the auxiliary panel of Fig. 8, the blue symbols are based on $F = 0.3\epsilon/\sigma$ on $\{i, j\} = \{43, 43\}$, and the red symbols are based on $F = 0.5\epsilon/\sigma$ on $\{i, j\} = \{15, 15\}$.

Finally, as mentioned earlier, experimentalists typically make measurements at a finite force, attempting to obtain an estimate for the free energy at $F = 0$. For such a task in the context of the activation energy, we consequently formulate an approximation that is similar to Eq. 17. By performing analogous mathematical manipulations as done in the context of Eq. 15, we obtain the following useful expression for force spectroscopy:

$$G_0^{\text{act}} \approx G_F^{\text{act}} + \left[\langle r_{ij} \rangle_F^{\ddagger} - \langle r_{ij} \rangle_F^{\mathcal{A}} \right] F - \frac{1}{2} \frac{1}{kT} \left[\langle \Delta r_{ij}^2 \rangle_F^{\ddagger} - \langle \Delta r_{ij}^2 \rangle_F^{\mathcal{A}} \right] F^2 + \ldots \tag{18}$$

16

In the top panel of Fig. 10, by invoking two sets of the Zwanzig data, at $F = 0.3\epsilon/\sigma$ on beads $\{43, 43\}$ and at $F = 0.5\epsilon/\sigma$ on beads $\{15, 15\}$, we respectively plot these estimates for the force-free scenario as blue and red (upwards and downwards) triangles respectively for the (first-order and second-order) approximations of Eq. 18. Just as in Fig. 8, the data points here do not demonstrate sufficient replication capabilities. We suspect that a decent amount of the error stems from the fact that the locations of the extrema shift with F. In any case, Eq. 18 still holds promise for experimentalists in estimating the force-free G_0^{act}, if they can make measurements for sufficiently weak forces.

9   *Relaxation Energy of the Crystal-Coil Transition*

Besides G_F^{act}, which has an intimate connection with the kinetics of unfolding, we can also evaluate the overall change in the free energy between the collapsed and expanded states; we call this the relaxation energy G_F^{rlx}: We depict it schematically in Fig. 5, and it is defined in an analogous manner as the activation energy of Eq. 16 (i.e., $G_F^{\mathrm{rlx}} = G_F\left(U^{\mathcal{B}}\right) - G_F\left(U^{\mathcal{A}}\right)$). In turn, the corresponding approximation of Eq. 17, as well as in Eq. 18, holds for any polymer: The sole difference is that the $\ddagger$ index must be replaced with the index of the unfolded state. Specifically for our polymer, we present its relaxation energy, together with its relevant approximations, in the bottom panel of Fig. 10, using here the same notation as in the respective top panel; this data is again for the $\{29, 29\}$ scenario. While this relaxation energy is a strictly different property than the activation energy, the interesting aspect in this graph is that it follows the same trend: G_F^{rlx} has a negative slope and a negative curvature as a function of the applied force. For the overall free energy as a function of the "contacts-number" (e.g., the curves of $G_F\left(U\right)$ in Fig. 5), we can consequently state that such a functionality is more or less expected across the entire order parameter in the proximity of $F = 0$.

Let us now discuss the ramification of these results. Foremost, an expression reminiscent of Eq. 17 for the relaxation energy has been derived in other works as well [9], but there is a special implication with the observations in this work: For a generic polymer that exhibits the crystal-coil transition with no specific preference between its contacts, its relaxation energy in force spectroscopy is always expected to exhibit a negative slope and a negative curvature in the vicinity of $F = 0$ (i.e., the red curve of Fig. 1). Of course, we made a similar statement for the activation energy, but we make a further claim for G_F^{rlx}: We actually expect such a trend for the unfolding of any protein. The reason for this stems in the moments of the bead-bead distance: Comparing a very rigid crystal and a very floppy coil, both relevant differences, between their means (i.e., $\left[\langle r_{ij}\rangle_0^{\mathcal{B}} - \langle r_{ij}\rangle_0^{\mathcal{A}}\right]$) and between their variances (i.e., $\left[\langle \Delta r_{ij}^2\rangle_0^{\mathcal{B}} - \langle \Delta r_{ij}^2\rangle_0^{\mathcal{A}}\right]$), will be strictly positive in the force-free limit (in consideration of Fig. 7), and thus, the functionality observed in Fig. 10 is expected regardless of the chemical peculiarities of the protein. Thus for the relaxation energy in the vicinity of $F = 0$, we cannot imagine the other options discussed in the previous section for G_F^{act} (i.e., the blue curve of Fig. 1); in other words, we expect only one functionality type for it.

17

10 *Conclusion*

In this work, with molecular simulations of the biomimetic polymer of Taylor et al. [17, 18], we have elucidated on the (generic) kinetic behavior of proteins in force spectroscopy. In particular, we showed that the free energy for the unfolding of an arbitrary chain (with no specific preferences among its beads) exhibits a characteristic signature in the vicinity of the force-free scenario: Above all, the activation energy has a negative slope and a negative curvature as a function of the applied force, and this is irrespective of the specific pair of monomers which are being pulled (note Figs. 9 and 10). While our molecular simulations are specific for the coexistence temperature between the crystal and coil phases, our Zwanzig-based formalism is completely general, and thus, we expect an analogous trend for any temperature that exhibits an activation barrier between these two metastable states. Regardless, the explanation for this behavior lies in the Taylor approximation of Eq. 17: The linear and quadratic terms in the series are respectively given by the means and the variances of the bead-bead distance, specifically evaluated as a difference of the transition region with respect to the folded state; in general, this distance is expected to have lower values, with lower fluctuations, in the folded state, and this in turn yields a negative slope and a negative curvature for the force functionality. We also derived here Eq. 18, which is applicable for any protein, and thus, it can be very useful for experimentalists: By measuring the first and second moments of the bead-bead distance at a finite force, one can make an approximation for the rate coefficient of the (intrinsic) force-free folding.

Considering that in reality residues have specific preferences for each other, force spectroscopy may of course exhibit other trends, especially if the pair being pulled has a unique role in the transition mechanism (note Figs. 1). Nevertheless, since the behavior of heterogeneous biological polymers is significantly influenced by the behavior of homogeneous generic polymers, we expect that the observations in our work hold for most residues in most proteins. This statement is in fact complementary with recent kinetic theories which also expect such a behavior for most proteins [9]. Note that this is in contrast with the Dudko formula, which presumes that the bead-bead distance is always the reaction coordinate for unfolding [11]. It has been suggested that while such an assumption is formally valid in the vicinity of the critical force at which the activation energy vanishes, it is usually incorrect in the vicinity of the infinitesimal force; in essence, there is a crossover in the reaction coordinate as the force increases [14, 15]. Specifically in our work, we argue that the distance between the monomeric pair cannot generally be the reaction coordinate in the force-free limit, since such an order parameter cannot even cleanly distinguish between the crystal and coil phases (note Fig. 4). For the intrinsic folding process, the number of contacts a chain makes with itself is a much better representation of the reaction coordinate [22, 23]. This is in fact the main assumption of our study, which is more or less validated by the likelihood investigation of Refs. [20, 21]. On a final note, the mere fact that we attain reminiscent trends as observed in kinetic studies of protein folding indicates that much of force spectroscopy may be simply understood in terms of equilibrium phenomena of generic polymers. Nevertheless, keep in mind that there are some aspects of protein folding which cannot be described by our generic chain: For example, intermediate states in the transition mechanism are typically observed during force spectroscopy for heterogeneous polymers, yet this aspect is absent for our homogeneous polymer [26, 27]. Besides, in describing the entire phase transition correctly for purposes of force spectroscopy, one must be also mindful of the kinetics associated with the experimental apparatus itself [28].

Conflicts of Interest

There are no conflicts to declare.

Bibliography

[1] K. A. Dill, S. B. Ozkan, M. S. Shell and T. R. Weikl, *Annual Review of Biophysics*, 2008, **37**, 289–316.

[2] D. Thirumalai, E. P. O'Brien, G. Morrison and C. Hyeon, *Annual Review of Biophysics*, 2010, **39**, 159–183.

[3] W. J. Greenleaf, M. T. Woodside and S. M. Block, *Annual Review of Biophysics and Biomolecular Structure*, 2007, **36**, 171–190.

[4] C. Bustamante, *Annual Review of Biochemistry*, 2008, **77**, 45–50.

[5] I. Schwaiger, C. Sattler, D. R. Hostetter and M. Rief, *Nature Materials*, 2002, **1**, 232–235.

[6] C. Cecconi, E. A. Shank, C. Bustamante and S. Marqusee, *Science*, 2005, **309**, 2057–2060.

[7] S. Garcia-Manyes, L. Dougan, C. L. Badilla, J. Brujic and J. M. Fernandez, *Proceedings of the National Academy of Sciences*, 2009, **106**, 10534–10539.

[8] J. A. Rivas-Pardo, E. C. Eckels, I. Popa, P. Kosuri, W. A. Linke and J. M. Fernandez, *Cell Reports*, 2016, **14**, 1339–1347.

[9] D. E. Makarov, *The Journal of Chemical Physics*, 2016, **144**, 030901.

[10] G. I. Bell, *Science*, 1978, **200**, 618–627.

[11] O. K. Dudko, G. Hummer and A. Szabo, *Physical Review Letters*, 2006, **96**, 108101.

[12] R. B. Best, E. Paci, G. Hummer and O. K. Dudko, *The Journal of Physical Chemistry B*, 2008, **112**, 5968–5976.

[13] B. Jagannathan, P. J. Elms, C. Bustamante and S. Marqusee, *Proceedings of the National Academy of Sciences*, 2012, **109**, 17820–17825.

[14] Y. Suzuki and O. K. Dudko, *Physical Review Letters*, 2010, **104**, 048101.

[15] P. I. Zhuravlev, M. Hinczewski, S. Chakrabarti, S. Marqusee and D. Thirumalai, *Proceedings of the National Academy of Sciences*, 2016, **113**, E715–E724.

[16] Z. Huang and R. Boulatov, *Pure and Applied Chemistry*, 2010, **82**, 931–951.

[17] M. P. Taylor, W. Paul and K. Binder, *Physical Review E*, 2009, **79**, 050801.

[18] M. P. Taylor, W. Paul and K. Binder, *The Journal of Chemical Physics*, 2009, **131**, 114907.

[19] F. Wang and D. P. Landau, *Physical Review Letters*, 2001, **86**, 2050–2053.

[20] C. Leitold and C. Dellago, *The Journal of Chemical Physics*, 2014, **141**, 134901.

[21] C. Leitold, W. Lechner and C. Dellago, *Journal of Physics: Condensed Matter*, 2015, **27**, 194126.

[22] L. Sun, J. K. Noel, J. I. Sulkowska, H. Levine and J. N. Onuchic, *Biophysical Journal*, 2014, **107**, 2950–2961.

[23] R. Berkovich, J. Mondal, I. Paster and B. J. Berne, *The Journal of Physical Chemistry B*, 2017, **121**, 5162–5173.

[24] R. W. Zwanzig, *The Journal of Chemical Physics*, 1954, **22**, 1420–1426.

[25] J. Luettmer-Strathmann and K. Binder, *The Journal of Chemical Physics*, 2014, **141**, 114911.

[26] C. Hyeon, G. Morrison, D. L. Pincus and D. Thirumalai, *Proceedings of the National Academy of Sciences*, 2009, **106**, 20288–20293.

[27] R. Berkovich, S. Garcia-Manyes, M. Urbakh, J. Klafter and J. M. Fernandez, *Biophysical Journal*, 2010, **98**, 2692–2701.

[28] M. Hinczewski, Y. von Hansen and R. R. Netz, *Proceedings of the National Academy of Sciences*, 2010, **107**, 21493–21498.